18th International Conference on Space Operations, Montreal, Canada, 26 - 30 May 2025.

SpaceOps-2025, ID # 24

Cislunar PNT (LPNT) Simulation and Modeling Tools for CONOPS and System Architecture Assessment

Catania Calavitta[a], Lauren Helt[a], Ashley Jubb[a], Erika Luz[a], Ren Padgett[a], XinXue Wang[a], Charles Lee[a*], Tien M. Nguyen[,b], Xin Tan[c], John D. T. Nguyen[c], Genshe Chen[c], Khanh K. Pham[d]

[a] *California State University, Fullerton, California, USA,*
[b] *The Aerospace Corporation, El Segundo, California, USA,*
[c] *Intelligent Fusion Technology, Germantown, Maryland, USA*
[d] *Air Force Research Laboratory, Albuquerque, New Mexico, USA*
***** Corresponding Author: *Charleshlee@fullerton.edu*

Abstract

Cislunar Communications Relay and Navigation Systems (LCRNS), PNT (position, navigation, and timing) satellites, and far-side lunar exploration are essential topics in the U.S. cislunar science and technology (S&T) strategy. In this paper, we discuss and present a MATLAB LPNT simulator that can select the best options for launching Planned LCRNS on the L2 Lagrange point orbiting the moon. Our simulation and modelling (M&S) approach leverages existing global navigation satellite systems (GNSS) to explore the possibilities of using these systems with L2-Halo LCRNS. As a starting point, the GNSS satellites implemented in the MATLAB simulator are GPS, Galileo, and QZSS. The simulator incorporated desired PNT system parameters for this L2-Halo orbit based on the selected GPS, Galileo, and QZSS datalinks to be received by LCRNS. We will also evaluate the possibilities of using selected GNSS satellite systems to provide PNT services to LCRNS. We aim to develop a decision support tool such as this LPNT simulator to explore the possibility of using existing GNSS as part of a future sustainable "cislunar ecosystem" with scalable and interoperable PNT infrastructure.

Keywords: Cis-Lunar PNT, Modeling & Simulation, CONOPS, System Architecture Assessment

1. Introduction

The space race of the 1950s established the United States as a world power capable of feats that were once thought impossible. In 2024, we are in a second space race focusing on sustained exploration to the far side of the moon and the lunar south pole. However, recent efforts from several countries to launch a far-side lunar mission have failed. These missions failed because once the rover landed on the moon, the team on Earth could not locate and communicate with it. To ensure future successful exploration, the US has developed cislunar S&T strategies to ensure that successful cislunar missions are planned. The US Department of Defence (DoD) cislunar strategy would define the military's primary objective to promote a safe and stable environment, with the secondary benefit of enabling or accelerating the development of civil and commercial cislunar space. A DoD cislunar strategy would define the military's primary objective to promote a safe and stable environment, with the secondary benefit of enabling or accelerating the development of civil and commercial cislunar space. The US has passed an initiative to create a dedicated LPNT to provide position, navigation, and timing to a future lunar and planned Mars spacecraft.

This paper discusses the IFT-CSUF team's approach to designing and developing a MATLAB LPNT simulator to evaluate potential cost-effective and operable alternative LPNT architecture solutions using existing GNSS infrastructure. Our MATLAB simulator can create a non-dedicated LPNT architecture, such as GNSS, and assess its PNT performance to provide navigation and timing for future lunar missions. Our M&S approach is to (i) use existing GNSS with a focus on GPS, Galileo, and QZSS databases, comprising 64 satellites, to build an information relay in which our earth-orbiting GNSS satellites could communicate with an LCRNS lunar orbit; (ii) explore several lunar orbits while considering many figures of merit and with a special focus on lunar far-side data collection before focusing on an L2 Halo orbit with a 9.7-day orbital period containing 10 LCRNS satellites; and (iii) After selecting a particular lunar system, calculations are performed to assess the potential for communication and the strength of connectivity between Earth-orbiting satellites and lunar satellites. To do the calculations, we create models to define dynamic, time-dependent signal-to-noise ratio (SNR) and link margin calculations. The simulator can also calculate associated Doppler shifts/Doppler rates and make a preliminary localization model to approximate the position of a future lunar

user terminal with minimal error. The calculation process used by the proposed MATLAB CPNT is outlined in Figure 1. This paper discusses an advanced LPNT simulator and its implications for the future possibility of a non-dedicated LPNT.

2. GLOBAL NAVIGATION SATELLITE SYSTEM: A FOCUS ON GPS, GALILEO, AND QZSS

GNSS is a broad conceptual umbrella term that covers all satellite navigation and positioning systems. GNSS is crucial for everything from navigating with our phones to tracking logistics globally. GNSS seeks to improve the accuracy of position, velocity, and time information to satisfy the needs of different fields. GNSS satellites orbit far from the Earth's atmosphere. GPS satellites orbit at an altitude of around 20,000 km. GNSS orbits are roughly circular, with high stability and accurate predictability. They belong to a class of MEO (Medium Earth Orbit) [2]. The Galileo satellites orbit at a slightly higher altitude, at around 23,000 km. The GNSS satellites of interest are GPS and Galileo, the primary constellations in orbit, and the regional system QZSS – each is managed by a different entity, all of which rely on satellite signals for positioning and navigational judgment [1].

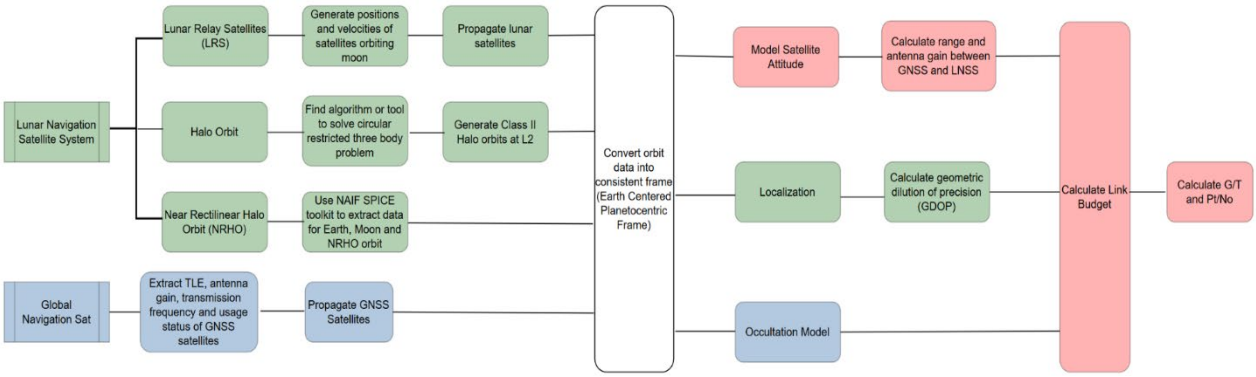

Figure 1: Calculation process describing the M&S models implemented in our MATLAB LPNT simulator.

Global Positioning System (GPS): GPS is a satellite-based navigation system owned and operated by the United States government. GPS provides accurate geographic location, vehicle speed, and precise time information anywhere in the world and near-Earth space [3]. The system comprises a constellation of at least 24 satellites orbiting the Earth at approximately 20,200 kilometers (~ 12,550 miles) above the surface. These satellites orbit the Earth in six orbital planes, with inclined orbits, to ensure global coverage. Each satellite completes an orbit every 12 hours.

Galileo: Galileo is the GNSS developed by the European Union (EU) and the European Space Agency (ESA). The Galileo constellation comprises 28 satellites orbiting the Earth at about 23,222 kilometers (about 14,429 miles). These satellites are distributed in three circular Medium Earth Orbit (MEO) planes, inclined at an angle of 56 degrees to the equator. Each Galileo satellite completes an orbit approximately every 14 hours and 7 minutes [4].

Quasi-Zenith Satellite System (QZSS): QZSS is a satellite-based augmentation system (SBAS) developed by the Japan Aerospace Exploration Agency (JAXA) to enhance the accuracy and availability of GPS signals in the Asia-Oceania region. The QZSS satellites operate at an altitude of approximately 36,000 kilometers (~ 22,369 miles) above the Earth's surface. Each QZSS satellite has a highly elliptical orbit of about 23 hours and 56 minutes, spending most of its time near Japan's zenith (directly overhead) [5].

Two-Line Element (TLE) Data: TLE data provides essential orbital parameters for each GNSS satellite, which is the "DNA" of satellite tracking. Every satellite has "NORAD_IDs" in the TLE data format, which is the unique identifier for each satellite, vital for tracking and avoiding collisions [10]. To understand the TLE data, we parse the HTML in MATLAB using the regular expressions (*regexp*) tool to extract all the GNSS sub-links with each satellite name of the TLE data. Segmentation through string processing and regular expressions provided the GNSS TLE data and processed the data into a usable format for this study. We obtained 31 GPS satellites, 28 Galileo satellites, and 5 QZSS satellites by extracting real-time satellite data. Five of the 28 Galileo satellites have been retired, 1 of the 5 QZSS satellites has been replaced, and only 4 QZSS satellites are in use.

TLE Propagator: MATLAB provides a TLE propagator code using the Eccentric orbit system to visualize the difference between the three propagator models. This propagator model showcases three orbit models: the Two-Body Keplerian, Simplified General Perturbations-4 (SGP4), and the Simplified Deep-Space Perturbations-4 (SDP4), each building on the previous model to include more variables and increasing accuracy [1]. The MATLAB propagator model is used as a base to create a propagator model for the selected GNSS orbit systems, including GPS, Galileo, and QZSS, using the SDP4 orbit model and the previously mentioned extracted TLE files. The SDP4 propagator model was chosen because it accounts for secular and periodic orbital perturbations caused by Earth's geometry, atmospheric drag, and solar and lunar gravitational force [1]. Within the model, the positions, velocities, start and stop times, and time step were recorded for each satellite in each GNSS system in the Geocentric Celestial Reference Frame and then extracted for frame manipulation [1]. Figure 2 illustrates simulation results for GPS, Galileo, and QZSS.

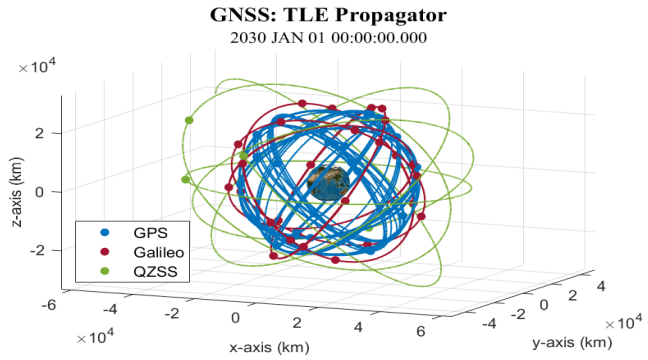

Figure 2: Still image of the TLE Propagator utilizing the three GNSS systems: GPS, Galileo, and QZSS.

3. CISLUNAR POSITION NAVIGATION AND TIMING (LPNT) M&S MODELS

Halo Orbits at Libration Point L2

The three-body problem is well-studied in physics. It helps to predict the trajectories of three objects of similar mass using the equations of motion and Newton's universal law of gravitation, given a set of initial conditions called state vectors.

$$\ddot{x} - 2\dot{y} - x = -\frac{(1-\mu)(x+\mu)}{d^3} - \frac{\mu}{r^3}(x - 1 + \mu) \qquad (3.1)$$

$$\ddot{y} + 2\dot{x} - y = -\frac{(1-\mu)}{d^3}y - \frac{\mu}{d^3}y \qquad (3.2)$$

$$\ddot{z} = -\frac{(1-\mu)}{d^3}z - \frac{\mu}{r^3}z \qquad (3.3)$$

The circular restricted three-body problem (CR3BP) is a special case of the three-body problem where one of the three objects' mass is negligible compared to the masses of the other two objects. It is the CR3BP that is used to find potential Halo orbits [6], [13]. Many functions are available to solve the CR3BP and are available for MATLAB and Python. However, many of these functions provided Halo orbits that contained pinch points, did not provide the entire trajectory of the orbit, or did not provide the feasibility of the Halo orbit. We need to find a reliable method for designing a Halo orbit because relying solely on these functions would be like working blindly.

The Jet Propulsion Laboratory (JPL) has a publicly available Halo orbit design tool that provides pre-computed periodic orbits around Libration points L1*, L2, and L3. JPL's Poincaré Periodic Orbit Database†, which relies on the CR3BP, provides low-energy periodic orbit trajectories [13, 14]. This tool filters for class II (southern-focused) Halo orbits around L2. Once filtered, a list of over 1,500 possible orbits is populated. These orbits include non-dimensional state vectors, Jacobi constant, orbital period, the JPL orbit ID, orbital period given in days, and the stability index. Of the 1,500 potential orbits, we decided to examine 12 orbits further. These orbits have periods ranging from 3 to 14 days, with one orbit increment in the orbital period for each day. The percentage of time that there are at least 4 GNSS

* Note that the L1 and L2 defined here are the Lagrange point 1 and 2 not the GPS frequencies L1 and L2.
† https://ssd.jpl.nasa.gov/tools/periodic_orbits.html#/intro

satellites given the LCRNS is calculated and compared alongside their stability index. Table 1, shown below, summarizes these L2 Halo orbits' characteristics.

Halo Orbits at L2 and Lunar Surface Coverage Analysis

The visibility of the Halo orbits at L2 from the surface of the Moon is examined to gather more information on which orbit period is the optimal choice. This analysis assumes that the frame was in the Earth-Moon Fixed Barycentric frame. The parameters established to represent the lunar surface were longitude and latitude coordinates ranging from -180° to 180° and -90° to 90°, respectively, with 10° increments. The Moon's Barycentric distance from the Earth was defined as 379,729.3155 km. The LCRNS were the satellites in Halo orbits at L2 from the 3.19 to 14.0-day periods. The formulations comprise the different areas on the surface of the Moon, Q , defined by,

$$Q = P + M \tag{3.3}$$

where P is the (x, y, z) equivalents of the longitude and latitude values of the Moon after conversion to Cartesian coordinates and M is the Moon's Barycentric distance from the Earth. Additionally, the angle θ between the vectors v and u is computed using:

$$\theta = cos^{-1}(u \cdot v);\ u = \frac{Q}{||Q||};\ v = \frac{s-Q}{||s-Q||} \tag{3.4}$$

The vector u represents the points on the Moon's surface relative to the Earth-Moon barycenter, s is the lunar satellite's position, and v is the position of the satellites relative to the Moon's surface. If the angle θ is less than or equal to 90°, the satellite is visible from the given coordinates.

After applying these formulations, one metric was gathered and used in the analysis to determine which orbit period to choose: the average number of satellites visible over time, which is in the fourth column of Table 1 (see below). Another metric recorded is the percentage of coordinates that can see at least four satellites over time, which can be found in the last column of Table 1.

Table 1. Summary of L2 Southern Halo Orbit Characteristics

JPL Orbit ID	Orbital Period (days)	Stability Index	Average No. Of Visible Satellites	Satellite Coverage (%)
1021	3.19	1.00	3.4891	47.37
954	4.01	1.00	3.6327	47.37
875	4.01	1.00	3.7944	50.15
759	6.00	1.00	3.9769	53.01
574	7.01	1.46	4.4478	55.80
400	8.06	1.69	4.6292	59.62
249	9.01	1.46	4.7255	62.36
129	9.77	1.00	4.7736	65.64
77	11.0	2.44	4.8340	74.85
266	12.0	8.77	4.8734	80.23
493	13.0	25.5	4.9060	81.99
680	14.0	86.0	4.9323	79.45

The importance of having at least four satellites in view lies in the requirement that, in the PNT formulations, three satellites are needed to solve for the unknown three-dimensional position of a receiver or user. In contrast, the fourth satellite corrects the clock offset or error [19]. The measurements we gathered are animated into dynamic heat map charts for 24 hours. Some are taken from these animations, as shown in Figure 3. The darkest blue color represents

zero visible satellites, and as the color changes to lighter shades up to yellow, it shows more visible satellites, with 10 being the maximum. The x-axis denotes the longitude values, while the y-axis shows the latitude values. The subtitle in blue shows the percentage of coordinates with at least four visible satellites at the given time, and below that, the text in black displays the average number of visible satellites over time for the given L2 Southern Halo Orbit Period.

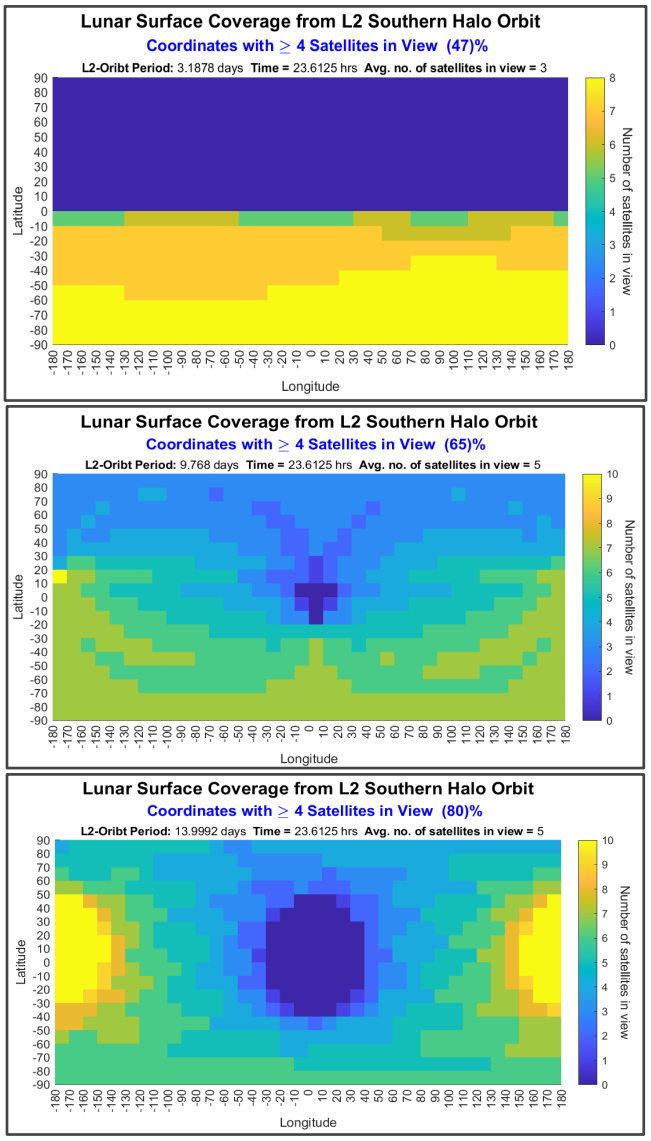

Figure 3: Still image from the dynamic heat map showing the number of visible satellites at time = 23.6125 hours for the satellites in Halo Orbits at L2 for 3.19 days (top), 9.77 days (middle), and 14.0 days (bottom).

Once the orbits are selected using L2 Southern Halo orbit characteristics shown in Table 1, they must be dimensionalized for use in the MATLAB LPNT simulator. This is done using dimensional analysis. The orbits are then plotted in the Earth-Moon Fixed Barycentric frame for comparison, as seen in Figure 4, with different views.

Our team also investigates another JPL orbit, namely JPL ID: 129. This orbit was chosen because it has the highest percentage of satellite coverage and the lowest stability index value. Finally, the orbit trajectory is converted to the Geocentric Celestial Reference frame.

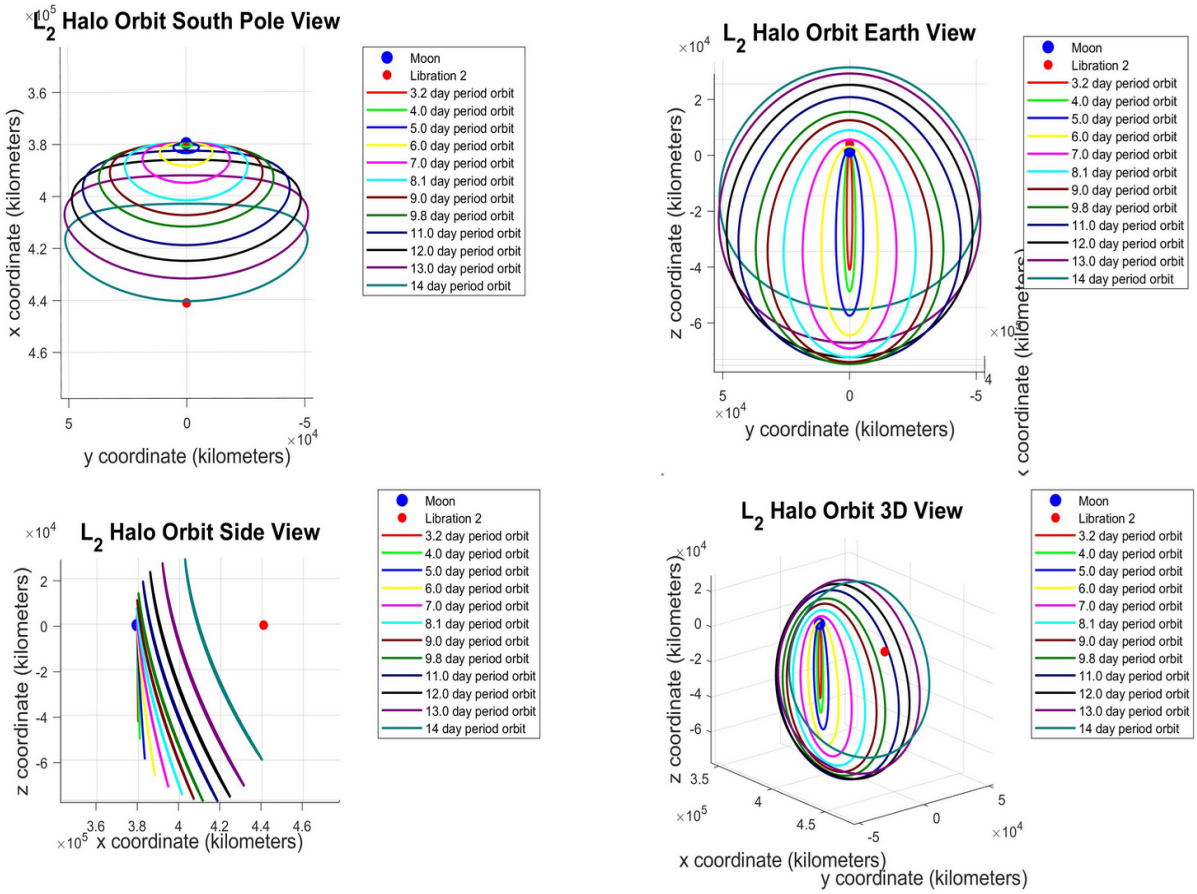

Figure 4: Different views of the selected L2 Halo orbits.

High Precision Lunar Orbit Propagator

Although we select the Southern (S) Halo Orbits at L2 (L2SHO), we also want to show that we can approximate the trajectories of a set of lunar satellites using a high-precision lunar orbit propagator. A high-precision lunar orbit propagator is a computational tool that accurately predicts the positions and velocities of satellites orbiting the Moon. What makes it highly precise is that it considers disturbances encountered by the satellites in its computations, such as solar radiation pressure, the gravitational pull of other bodies, and the lunar gravitational harmonics model. We leverage MATLAB's toolboxes, namely Simulink, Aerospace Blockset, and Aerospace Toolbox, to perform the propagation [8]. The necessary inputs are the six orbital elements of the satellites, and the output of the propagator is the positions and velocities of the satellites. The information required to perform the propagation is the six orbital elements of a satellite: semi-major axis, eccentricity, inclination, right ascension of the ascending node, the argument of periapsis, and the true anomaly. In addition, the required inputs are the start date, duration, orbit type, central body, output frame, propagator type, gravity model, Moon spherical harmonic potential model, spherical harmonic model degree and order, and the solver type.

The set of lunar relay satellites we propagated is adapted from ESA's Moonlight Navigation Satellite System. ESA's Moonlight initiative aims to create and develop specialized lunar communication and navigation services to strengthen current and future lunar exploration missions [5]. These five satellites were described to be in elliptical lunar frozen orbits, meaning that relative to the Moon, the positions of the satellites are relatively stable over time. A recent study by JPL also used three satellites in ELFO, which are added to the satellites propagated [7]. This resulted

in 8 satellites in the Elliptical Lunar Frozen Orbit (ELFO). The parameters set to run the propagator are shown in Table 2.

Table 2. High Precision Lunar Orbit Propagator Parameters

Semimajor Axis (SMA)	[9750.7, 9750.7, 9750.7, 9750.7, 9750.7, 9750.7, 6053.47, 6053.47, 6053.47] (km)
Eccentricity	[0.7,0.7,0.7,0.7,0.7,0.594114,0.594114,0.594114]
Inclination	[63.2°,63.2°,63.2°,63.2°,63.2°,57.6995°,57.6995°,57.6995°]
The right ascension of the ascending node	[0°,120°,240°,120°,240°,0°,120°,240°]
Argument of periapsis	90°
True anomaly	[0°,164°,196°,245°,184°,0°, 159.6°,201.4°]
Start date	January 1, 2030
Duration	24 hours
Orbit type	Keplerian
Central body	Moon
Output frame	Moon-centered fixed coordinate frame
Propagator type	Numerical (high precision)
Gravity model	Spherical Harmonics
Moon spherical harmonic potential model	LP-100K
Spherical harmonic model degree and order	100
Solver type	Fixed step

4. REFERENCE FRAME TRANSFORMATIONS

Reference frames are fundamental to understanding the geometry and kinematics of satellite orbits. These frames are defined by three mutually orthogonal, unit-length direction vectors. In our study, we use two distinct reference frames: (i) the Earth-Moon (EM) System and (ii) the Geocentric Celestial Reference System (GCRS).

Earth-Moon (EM) System

For simulating the L-2 Southern Halo Orbit (L2SHO), we use the Earth-Moon Rotating Frame (EMRF), a non-inertial, rotating frame. At the center of this frame lies the Earth-Moon barycenter. The X-axis is oriented along the instantaneous Earth-Moon position vector, the Z-axis is aligned with the angular momentum vector, and the Y-axis is defined as the cross-product of the Z-axis and the X-axis. The JPL Orbital Tool Kit was employed to propagate the orbits in this frame.

Geocentric Celestial Reference System (GCRS)

The GNSS satellites are propagated in the GCRF, an inertial, non-rotating frame centered at Earth's center of mass. This frame is the Earth-centered realization of the International Celestial Reference Frame (ICRF). This equatorial coordinate system has its X-axis aligned with the celestial equator defined by the mean equinox of Earth at noon Terrestrial Time on January 1st, 2000. The Z-axis aligns with the Earth's rotation axis, the celestial pole. The Y-axis completes the orthogonal system and is defined as the cross-product of the Z-axis and the X-axis.

Frame Transformation

Before analysing LPNT possibilities between the L2SHO and GNSS satellites, we must transform the L2SHO to the Geocentric Celestial Reference Frame. Before applying coordinate rotations, the L2SHO satellites were shifted to align with the origin at Earth’s center of mass. This was a single linear translation of the x-position components.

$$Psat_{EM} = Psat_{EM} - [4671, 0, 0]^T \qquad (4.1)$$

For the sake of simplicity in the equations to come, $Psat_{EM}$ will refer to the Earth-centered positions of the L2SHO as stated in Eq. (4.1). To manage transformations between these frames, we utilize NASA's Navigation and Ancillary Information Facility (NAIF) SPICE Toolkit. NAIF provides high-precision observation geometry and user-level software for planetary analysis [19]. Our research requires explicit ephemeris data for the Moon and Earth, extracted from NAIF, to construct the frame transformation for the L2SHO satellites to the GCRS.

The transformation process involves using the Moon's position relative to the origin in the Earth Mean Equator J2000 (EME2000) frame, extracted with SPICE frame ID "J2000". At each time step, t, we define the coordinate axes as follows: the X-axis is the normalized Earth-to-Moon position vector $Pm_{J2}(t)$, the Z-axis is the normalized cross-product between two consecutive position vectors, and the Y-axis is the cross-product of the Z-axis and the X-axis. These (x, y, z) vectors represent axes (i, j, k) in the following equation, respectively.

$$\hat{\imath} = \frac{P\vec{m}_{J2}(t)}{\|P\vec{m}_{J2}(t)\|} \qquad \hat{k} = \frac{P\vec{m}_{J2}(t-1) \times P\vec{m}_{J2}(t)}{\|P\vec{m}_{J2}(t-1) \times P\vec{m}_{J2}(t)\|} \qquad \hat{\jmath} = \hat{k} \times \hat{\imath} \qquad (4.2)$$

The following equations define the L2SHO satellite positions and velocities in the inertial Earth-centered coordinates within the EME2000 frame. All calculations use right-handed Cartesian coordinates.

It should be noted that the EME2000 frame in SPICE documentation coincides almost precisely with the realization of ICRF, with differences being a rotation of less than 0.1 arcsecond. [9]. We apply a final rotational matrix transformation to both satellite systems to ensure the exact alignment of the frame and coordinate systems of the L2SHO to the GNSS satellites. This rotation specifically accounts for polar offset at the desired simulation times (January 1st to January 2nd, 2030) by using the right ascension (RA) and declination (DEC) of Earth's pole. Declination measures the angular distance north or south of the celestial equator, analogous to terrestrial latitude. In contrast, right ascension measures the eastward angular distance along the celestial pole, analogous to terrestrial longitude.

The RA and DEC are calculated using the ephemeris time associated with each time step in our simulations. Using NAIF SPICE functions, this was converted to Julian centuries past the J2000 epoch, defined as $J(t)$ in the following equations.

$$RA(t) = 0.0 - 0.641 * J(t)$$

$$DEC(t) = 90.0 - 0.557 * J(t) \qquad (4.3)$$

These two angles, defined in degrees, are then used to create a combined rotation matrix to apply to the positions and velocities of all satellites at each time step. Eq. (4.4) uses a general vector $[Px, Py\ Pz]^T$ to represent the rotation applied to both GNSS and L2SHO satellites. This was similarly done with the velocity vectors $[Vx, Vy\ Vz]^T$ associated with each position.

$$\begin{bmatrix} P'_x \\ P'_y \\ P'_z \end{bmatrix} = \begin{bmatrix} \cos(RA^\circ)\sin(DEC^\circ) & \sin(DEC^\circ)\sin(RA^\circ) & -\cos(DEC^\circ) \\ \sin(RA^\circ) & \cos(RA^\circ) & 0 \\ \cos(DEC^\circ)\cos(RA^\circ) & \cos(DEC^\circ)\sin(RA^\circ) & \sin(DEC^\circ) \end{bmatrix} * \begin{bmatrix} P_x \\ P_y \\ P_z \end{bmatrix} \qquad (4.4)$$

This concludes the frame transformations needed to define both satellite systems in the same Earth-centered inertial frame. This allows us to use their positions and velocities for satellite communication analysis.

5. OCCULTATION MODEL

Using the TLE files extracted earlier in the research process, an occultation model shows the line of sight (LOS) between the GNSS and LCRNS satellites. An occultation occurs when an orbiting object breaks the line of sight between a target body and an observing body [15]. For this study, the target/observer bodies are the GNSS and LCRNS

satellites, while the orbiting objects are the Earth and the Moon. For example, if a satellite in the Galileo system were to orbit behind the Earth, it would have no LOS to the satellites in the L2-Halo satellite system of the Moon. Thus, the model is occulted.

To visualize this occultation process, the model shown in Figure 1 is built considering all 3 GNSS systems and all 10 LCRNS satellites, as well as visualizing the communication between LCRNS and GNSS by observing the number of communications between each satellite in GNSS and LCRNS on L2SHO. The model is designed and developed to first output a data matrix containing binary data for the occultation, where 0 represents no LOS and 1 represents an LOS between each GNSS and LCRNS satellite. The binary values are determined by finding if the distance between a body-centered point *P* is greater than the body's radius *R*. Using the diagram shown in Figure 5 and Equations 5.1, 5.2, 5.3, and 5.4, if the minimum squared distance of point *P* and point *Q* is greater than the squared radius $R^2$of the body, then the binary output would be 1. On the other hand, if the minimum square distance is less than the squared radius R^2 then the binary output will be 0.

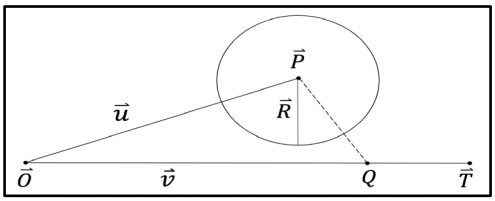

Figure 5: Geometry visualization of occultation model.

$$Q = \vec{O}\text{-}t\vec{V} \qquad \vec{u} = \vec{P} - \vec{Q} \qquad \vec{v} = \vec{T} - \vec{O} \tag{5.1}$$

$$SqDist(t) = \langle\vec{u},\vec{u}\rangle - 2t\langle\vec{u},\vec{v}\rangle + t^2\langle\vec{v},\vec{v}\rangle \tag{5.2}$$

$$t^* = \frac{\langle\vec{u},\vec{v}\rangle}{\langle\vec{v},\vec{v}\rangle} \tag{5.3}$$

$$minSqDist = \langle\vec{u},\vec{u}\rangle - \frac{\langle\vec{u},\vec{v}\rangle^2}{\langle\vec{v},\vec{v}\rangle} > R_p^2 \tag{5.4}$$

The binary matrix was then used as input for an animation model that connects each satellite within a GNSS system and an LCRNS system with a bright green line if the two satellites have an LOS, if the binary output is 1. For simplicity of the animation with a still image shown in Figure 6, only the Galileo and L2-Halo orbit systems are displayed. However, the systems can be interchanged as desired.

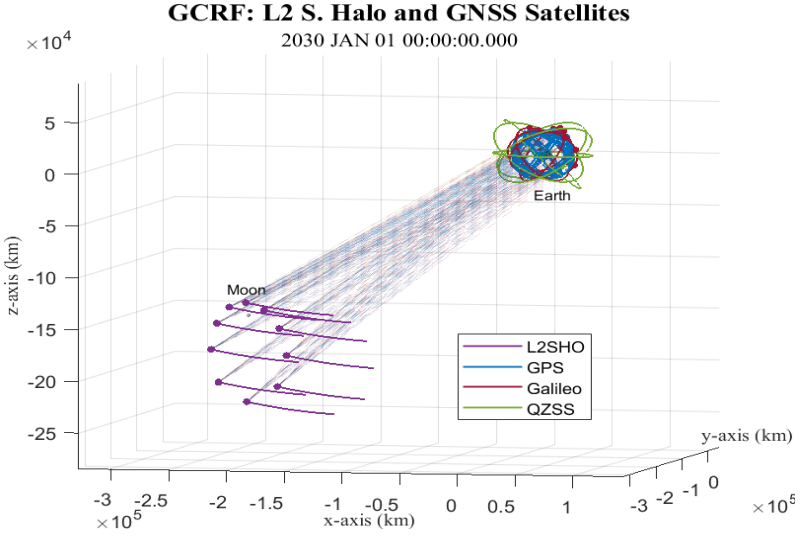

Figure 6: Still image of the LOS model between Galileo and L2.

Figure 7 shows the simulation results for L2SHO with days for GPS, Galileo, and QZSS satellites within the field of view (FOV) (a.k.a. LOS) of an LCRNS orbiting the Halo orbit. The simulation results show that, on average, there will be around 40 satellites out of 64 GNSS satellites from GPS, Galileo, and QZSS.

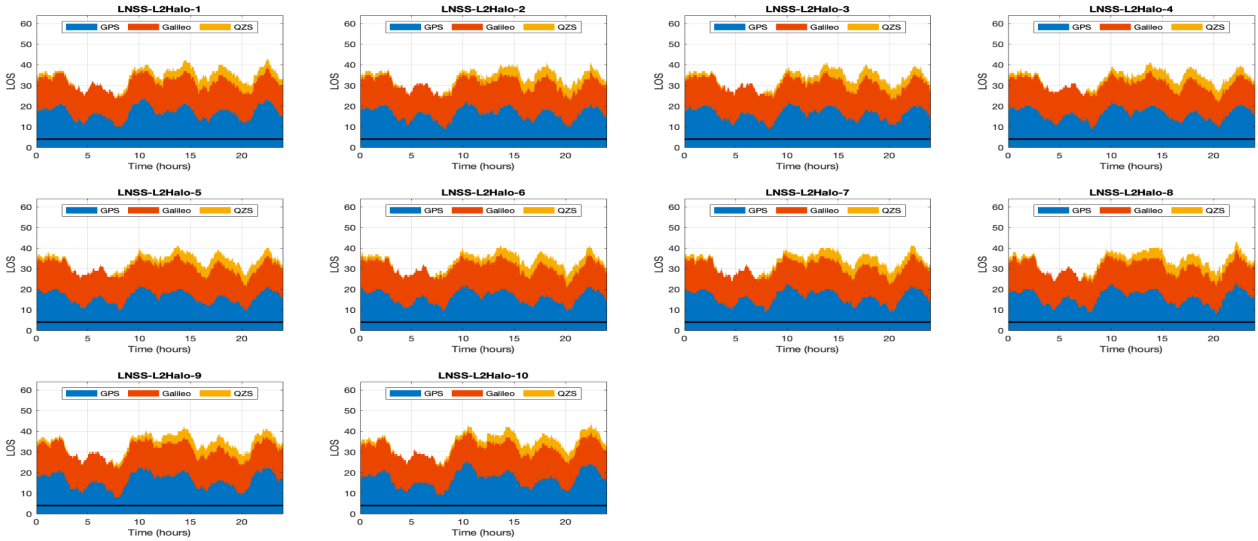

Figure 7: Number of GPS-Galileo-QZSS satellites in view with L2 S. Halo 9.7-day-period orbits.

6. DOPPLER MEASUREMENTS

Doppler shifts are the observed change in signal frequency from the transmitted frequency because of the relative motion between the satellite and the receiver. Doppler rates, which represent the rate of change of the Doppler shift, are approximated using numerical differentiation methods, specifically the second-order finite differences technique.

The practical significance of analyzing Doppler shifts/ Doppler rates lies in their ability to enhance the PNT accuracy of satellite-based systems. Understanding the Doppler effects in satellite communication is essential for compensating for frequency shifts to maintain clear and stable communication channels. This phenomenon is critical for accurately determining the relative velocity of satellites, which is pivotal for PNT services and for maintaining robust communication links.

For our calculations, we use a transmitter frequency (f_0) of 1575.42 MHz, which corresponds to the L-1‡ frequency band of the GNSS satellites. We defined the 64 GNSS satellites as the transmitters of the 10 L2SHO satellites observed.

The L2SHO are referred to as the receiving satellites or user satellites. Regarding the Doppler shift equation S denotes the GNSS state vector (position and velocity vector) and U denotes the L2SHO state vector. The shifts are calculated between each satellite in the two systems at every time step, resulting in a three-dimensional matrix of the form $(64, 10, Nt)$, where Nt is the number of time steps. To analyze the Doppler shifts and rates, we conduct two computer simulations using the following Doppler Shift equation:

$$\Delta\vec{v} = \vec{U}_v(t) - \vec{S}_v(t + lt)$$

$$\Delta\vec{p} = \vec{U}_p(t) - \vec{S}_p(t + lt) \qquad (6.1)$$

‡ To avoid confusion with Lagrange points L1 and L2, we denote GPS/QZSS L1 and L2 frequencies by L-1 and L-2 frequencies in this paper.

Δp and Δv are defined by the difference between the positions and velocities, respectively, between the user satellites, U and the observed satellites, S, adjusted for light time delay, is denoted as lt in the following equations. The speed of light is represented by c.

$$lt = \frac{\vec{U}_p(t) - \vec{S}_p(t)}{c} \qquad (6.2)$$

The first simulation below used the previously defined time frame of 24 hours with a time step of 5 seconds. This coarse resolution helps track satellite movements and observe range fluctuations over an extended period. Understanding these fluctuations is crucial for satellite tracking, as it helps predict satellite positions and maintain precise orbits. This longer-duration simulation allows for monitoring changes in the Doppler shift that can indicate shifts in satellite trajectories or unexpected orbital changes. Figure 8 shows the simulation results of the Doppler Shifts between the first L2 S. Halo Satellite and the 64 GNSS satellites.

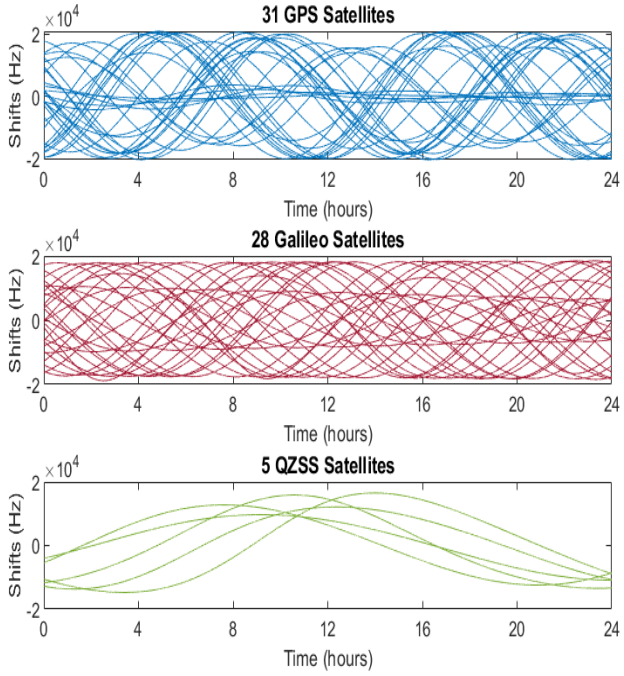

Figure 8: Doppler Shifts Simulation between the first L2 S. Halo LCRNS Satellite and the 64 GNSS satellites, GPS (top), Galileo (middle), QZSS (bottom).

The second simulation spanned a shorter duration of 20 seconds with finer time steps of 1 millisecond, 5 milliseconds, and 10 milliseconds. This high temporal resolution is needed for applications such as precise PNT services and communication relays. Accurate Doppler measurements at fine time steps enable better resolution of rapid changes in satellite velocity and position, essential for high-precision navigation and ensuring the reliability of communication links. As seen in Figure 9, the Doppler rates at these time steps result in calculation errors because of the small changes in values between each time step.

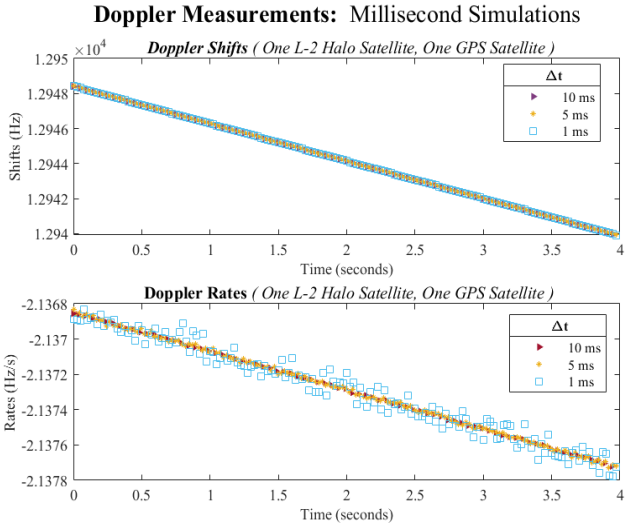

Figure 9: Doppler shifts (top) and Doppler rates (bottom) between the first L2 S. Halo LCRNS satellite and the first GNSS satellite (GPS sat#1), shown for the first 4 seconds of the simulation.

7. LINK BUDGET

The link budget accounts for all the power gains and losses of a communication signal between GNSS and LCRNS. With our non-dedicated cislunar PNT, the goal of the link budget is to model dynamic SNR and link margin calculations between the 64 GNSS satellites and each of the 10 L2SHO LCRNS satellites.

Projection of Satellite Orientation Vectors onto LOS

The first step in calculating the link budget is to obtain the azimuth and off-boresight angles to determine the attitude and position of the GNSS satellites regarding the L2SHO. This is computed by projecting the orientation vectors associated with each GPS, Galileo, and QZSS satellite onto the LOS between the GNSS and L2SHO LCRNS satellites. These projections are calculated using 3-dimensional calculus as follows:

$$\left(u_x, u_y, u_z\right) = \left(\langle \overrightarrow{LG}, x\rangle, \langle \overrightarrow{LG}, y\rangle, \langle \overrightarrow{LG}, z\rangle\right) \qquad (7.1)$$

where $u = LOS$, and $\overrightarrow{LG} = LNSS_p - GNSS_p$.

The (x, y, z) components of the satellites are converted into spherical coordinates to discern the azimuth and off-boresight angles with respect to the L2SHO. The conversion, moderated to reflect satellite position, are:

$$\phi(t) = \tan^{-1}\left(\frac{u_y(t)}{u_x(t)}\right) \qquad (7.2)$$

Interpolation of Existing GNSS Transmit Frequencies

Using existing antenna patterns, a two-dimensional linear interpolation is applied to these azimuth and off-boresight angles. The resulting time-dependent antenna gains are used as the transmitting antenna gain pattern for the L2SHO.

Transmission Powers and Frequencies

GNSS satellites transmit signals across various frequency bands, with L-band and E-band, each serving specific purposes crucial for navigation, positioning, and timing applications. Table 3 summarizes GNSS transmission frequencies for GPS, Galileo, and QZSS.

Transmit power is the amount of power emitted by a GNSS satellite to transmit a signal to a receiver on Earth, which directly affects the strength of the GNSS signal received by the receiver. Increased transmit power typically leads to stronger signals, improving receiver sensitivity and accuracy. However, more power means more precise signals at longer distances, but with that comes higher energy costs. Table 4 captures the GNSS transmission power for GPS, Galileo, and QZSS.

Table 3. GNSS Transmission Frequencies [17, 18]

Satellite Name	Type of Frequency	Type of Frequency
GPS/QZSS	L-1	1575.42 MHz
	L-2	1227.60 MHz
	L5	1176.45 MHz
Galileo	E1	1575.42 MHz
	E5a	1176.45 MHz
	E5b	1207.14 MHz
	E6	1278.75 MHz

Table 4. GNSS Transmission Power [17, 18]

Satellite Name	SVN Name	TX Power(watts)
QZSS	001,005	244
	002,004	500
	003	550
GPS	43,45,52,56,59,61	60
	48,50,52-55,57,58	145
	62-73	240
	74-79	399
Galileo	E101-102	135
	E103	95
	E104	160
	E105-224	265

Link Budget Calculation

Once the calculations for the dynamic range, transmitting gains from the GNSS to the L2 Halo orbit, and transmission powers are considered, a complete link budget is constructed between each transmitting GNSS and receiving L2SHO LCRNS satellite. Figure 10 captures a set of notional link budget parameters used to determine the SNR and link margin between each satellite, assuming the most advanced coding type for the navigation signal. The assumed parameters used for the calculations are a receiving gain of 38 dBi, an L-1 carrier frequency of 1575.42 dB-Hz, and the data rates and coding gain of 100 bps and 11 dB, respectively. The transmit gain for a user on the Earth is gathered by extracting the maximum value from the interpolated gains to reflect a gain closest to the Earth. To determine a dynamic link margin calculation, we consider single instance cases of our link budget and moderate the equation depending on the GNSS and L2SHO satellites in consideration. The calculation is as follows:

$$M_t = M_0 + \left(G_T - G_{T_0}\right) - 20\log_{10}\frac{d}{d_0} + \left(P_T - P_{T_0}\right) \qquad (7.2)$$

where Mt is the time-dependent margin, M0 is a margin using the single-instance base-line case, GT and GT0 are the time-dependent antenna gains and base-line case transmit gain, d and d0 are the range between the GNSS and lunar orbit, and PT and PT0 are the respective transmit powers.

For the GNSS and L2SHO LCRNS satellite systems to communicate, the communication must be within a certain threshold or margin. Links that we consider closed are those with a margin greater than or equal to 6 dB; see Figure

10 for the notional link parameters used in our simulation. Figure 11 shows the simulation results for the number of closed data links from the three GNSS systems to 10 L2SHO LCRNS satellites on L2 S. Halo orbit. The results look promising because the average number of closed links exceeds 4 dB. The calculation of SNR, which characterizes an antenna's performance, follows a similar approach to the link margin calculation. When evaluating the results of these figures of merit, we believe that using a non-dedicated PNT, such as GNSS, for future LPNT applications, with adjustments to the LCRNS satellite's hardware and software, may become a reality.

Data entry in Yellow cells	Tx = QZSS, Rx = User on Earth	Tx = QZSS, Rx = L2Halo	Variable	Units	Equation
Transmit Power (Tx Power)	244	244	P_{TW}	W	
Transmit Power (Tx Power)	23.87389826	23.87389826	P_T	dBW	$P_T = 10\log_{10}(P_{TW})$
Transmit Losses (cable, etc.)	0	0	L_T	dB	
Transmit Antenna Gain (Tx Gain)	16.294	-10	G_T	dBi	
Net Transmit EIRP	40.16789826	13.87389826	$EIRP$	dBm	$EIRP = P_T + L_T + G_T$
Carrier Frequency	1575.42	1575.42	f_0	MHz	
Transmit/Receiver Range	25,000	450,000	d	km	
FREE SPACE Path Loss	-184.3484995	-209.4539496	L_{FS}	dB	$L_{FS} = -20\log_{10}(4\pi f_0 \cdot 10^6/3 \cdot 10^5 \cdot d)$
Atmoshperic Loss	-2	-2	L_{ATM}	dB	
Polarization loss	-0.5	-0.5	L_P	dB	
Total path loss	-186.8484995	-211.9539496	L_T	dB	$L_T = L_{FS} + L_{ATM} + L_P$
Receive Antenna Gain	38	38	G_R	dBi	
Receive Losses (cable, etc.)	0	0	L_R	dB	
Tracking Loss (dB)	0	0	L_{TL}	dB	
Received Signal Power, Pt	-108.6806012	-160.0800513	P_R	dBm	$P_R = EIRP + L_T + G_R + L_R + L_{TL}$
Receive System Noise Figure	2	2	NF	dB	
System Noise Temperature	298.15	400	NT	K	
Ambient Noise Temperature				K	
Boltzmann's Constant x 290 K	-173.856861	-172.5806092	k	dBm/Hz	$k = 10\log(k \cdot NT/10^3)$
Carrier Power to Noise Power Spectral Density: Pt/No	65.17625981	12.50055793	SNR	dB/Hz	$SNR = P_R - k$
Data Rate	100	100		bps	
Data Rate	20	20	D_R	db-Hz	
Coding gain	11	11	G_C	dB	
Eb/N0 Achieved	56.18	3.50	$EbN0$	dB	$EbN0 = SNR - D_R + G_C$
Eb/N0 Required for BER = 1e-5	9.6	9.6	$EbN0_R$	dB	
Link Margin	**46.58**	**-6.10**	M	**dB**	$M = EbN0 - EbN0_R$

Figure 10: Notional link budget parameters

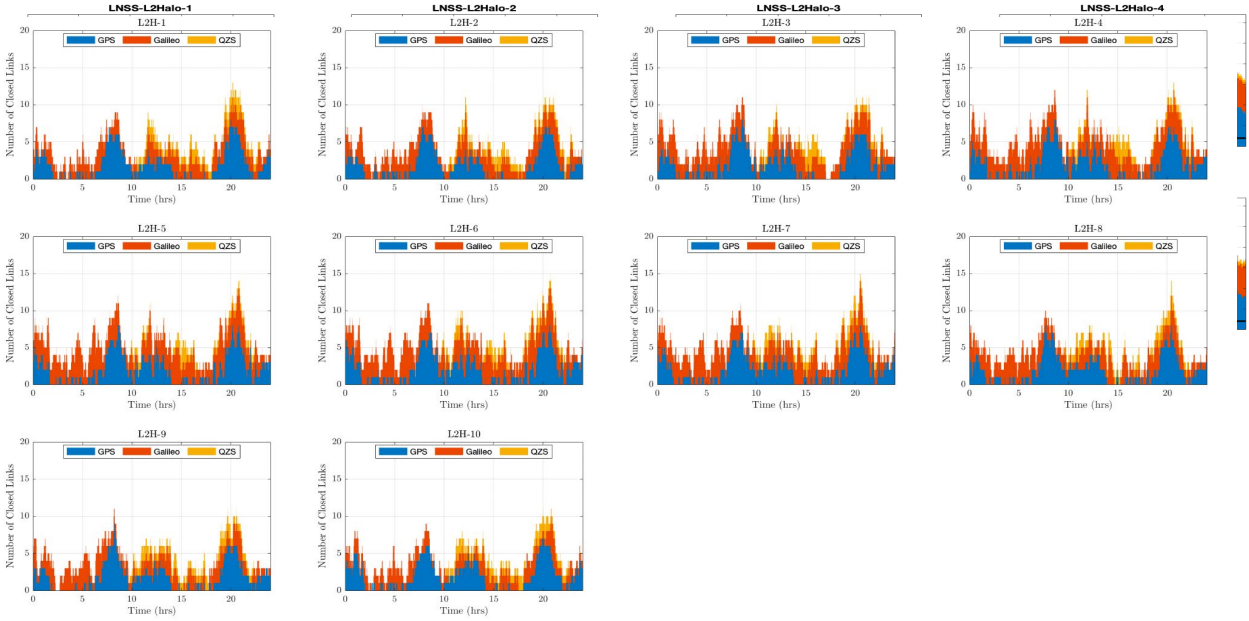

Figure 11: Number of GNSS satellites in a 24-hour period with the data links closed at least with a 6dB margin.

8. LOCALIZATION

Mathematical formulations are generated to approximate the user's position on L2SHO and the surface of the Moon for Moon lander missions, specifically at the lunar south pole, communicating with the chosen L2SHO period. The pseudo-range measurements, ρ, is computed using:

$$\rho_i^j(t) = \left|\left|x_i - s_j\right|\right| + cb_i + \mathcal{E}_i^j \quad (8.1)$$

where x_i is the user's coordinates, s_j represents the j^{th} satellite's coordinates, c is the speed of light, b_i is the i^{th} clock bias depending on the selected local oscillator (LO) device, $\mathcal{E}_i^j$ is the position error term depending on SNR and,

$$\left|\left|x_i - s_j\right|\right| = \sqrt{(x_i - x_j)^2 + (y_i - y_j)^2 + (z_i - z_j)^2} \quad (8.2)$$

(x_i, y_i, z_i) is the unknown position of the lunar user while (x_j, y_j, z_j) is the known satellite position. Linearizing the relationship between the pseudo-range measurements and the user's position vectors was expressed as follows:

$$F = Gx \quad (8.3)$$

where F is represented by a vector of adjusted pseudo-range measurements,

$$f_j(x_i) = -\rho_i^j(t) + \left|\left|x_i - s_j\right|\right| + c\widehat{b_i} \quad (8.4)$$

G is the Jacobian matrix.

$$G = \left[\frac{\partial f_j}{\partial x}_{Nx1} \quad \frac{\partial f_j}{\partial y}_{Nx1} \quad \frac{\partial f_j}{\partial z}_{Nx1} \quad \frac{\partial f_j}{\partial b}_{Nx1}\right] \quad (8.5)$$

where $j = 1, \ldots, N$ with N representing the number of satellites in view with the user and $x_i = [x_i, y_i, z_i, b_i]^T$ is the vector consisting of the unknown receiver position and clock bias. The formulas for each column in Eq. (8.5) can be expressed as

$$\frac{\partial f_j}{\partial x} = \frac{x_i - x_j}{\left\|x_i - x_j\right\|} \; ; \quad \frac{\partial f_j}{\partial y} = \frac{y_i - y_j}{\left\|y_i - y_j\right\|} \; ; \frac{\partial f_j}{\partial z} = \frac{z_i - z_j}{\left\|z_i - z_j\right\|} \; ; \frac{\partial f_j}{\partial b} = 1 \qquad (8.6)$$

Newton-Raphson Method

To solve for an approximation of the user's position, the aim is to find x_i such that $f_j(x_i) = 0$ for all visible satellites $j = 1, \ldots, N$ using the Newton-Raphson method. Starting with an initial guess for x_i, the method allows for iteratively finding an improved guess using the Jacobian matrix. Eq .(8.3) is solved by the following equation:

$$x_i^{(n+1)} = x_i^{(n)} - (G^T G)^{-1} G^T F \qquad (8.7)$$

after n iterations. The initial guess produces a random value between 0 and 2π for the azimuth, a random value between $-\frac{\pi}{2}$ and $\frac{\pi}{2}$ for the elevation and the Moon's radius. These are then converted to Cartesian coordinates. The guess is updated in each iteration, and the error is calculated. After several steps, the result is a more accurate approximation with a minimized error.

Geometric Dilution of Precision (GDOP)

The GDOP is used to assess how the geometric arrangement of the satellites affects the user's position localization calculations. When satellites are orbiting too closely together, the user's position estimate is less precise, resulting in a poor GDOP. When the satellites are spread apart, a higher-quality position approximation is produced, which is recognized as a good GDOP [11]. The GDOP value was used in this project to assess the localization formulations used to estimate the lunar user's PNT.

$$GDOP = \sqrt{tr(GG^T)^{-1}} \qquad (8.7)$$

Monte Carlo Simulation

The Monte Carlo method was incorporated to perform the localization for different circumstances. This is applied by localizing 1000 times within each time step (of every 5 seconds for 24 hours), resulting in different "testing" values for the satellite and pseudo-range noises (related to position error), clock error, and random values in the initial guess of the Newton-Raphson method. The metrics recorded and analyzed are the average GDOP value and the standard deviation of the errors.

Table 5. Localization Model Parameters for Testing

User's true position	[0; 0; r=-1737.4 (km)] (lunar south pole) r = moon's radius
LCRNS	L2 Southern Halo Orbits 9.7680 day period
Initial guess (θ, φ, r) - converted to Cartesian coordinates	Azimuth (θ): random value between 0 and 2π
	Elevation (φ): random value between -$\pi/2$ and $\pi/2$
	Radius (r): moon's radius
	Clock bias (b): random number
Monte Carlo runs	1000
Clock errors	[1; 10; 100] (nanoseconds)
Satellite position errors	[0.02; 0.2; 2] (kilometers)

Assumptions

We want to emphasize that the localization algorithm built for this project has not accounted for time dilation and the signal band-limiting effect. Furthermore, the parameters summarized in Table 5 are used to assess the quality of the L2SHO orbital model, mainly consisting of test parameters rather than actual data, especially the error values. These parameters are not used to measure errors but to evaluate potential PNT localization performance models.

Simulation Results

The localization performance model is evaluated for the estimation of the lunar surface user's position [0; 0; r =-1737.4 km] (lunar south pole) using the testing parameters in Table 5, and the measures used to analyze the results were the standard deviation of the user position errors and the GDOP values. The standard deviation position errors, specifically the σ, 2σ, and 3σ position errors, are illustrated in Figure 12. The x-axis denotes time, the left y-axis represents position errors in centimeters, and the right y-axis shows the number of visible satellites. The blue, yellow, and green lines represent the σ, 2σ, and 3σ values of the position error, respectively, while the orange line represents the number of visible satellites at each given time. The first column refers to scenarios with a clock error of 1 nanosecond, the second column to scenarios with a clock error of 10 nanoseconds, and the last column to scenarios with a clock error of 100 nanoseconds[§]. The first row depicts cases with a satellite position error of 0.02 km, the second row 0.2 km, and the third row 2 km. The plots show that when a satellite goes out of view from seven to six visible satellites, the σ, 2σ, and 3σ increase significantly. As the testing parameter for the satellite position and clock errors increases, the σ, 2σ, and 3σ errors also increase. This tells us that the localization model is sensitive to the number of visible satellites, and its accuracy is affected as the clock and satellite position errors increase.

The GDOP values obtained from the testing can be found in Figure 13. In all the different cases, the GDOP value is the same. Like the results of the σ, 2σ, and 3σ position errors, the GDOP significantly increases as a satellite goes out of view from seven to six satellites. Again, this shows that the number of visible satellites significantly affects the localization calculations. The geometric arrangement of the satellites appears to weaken since the GDOP values increase when fewer satellites are visible.

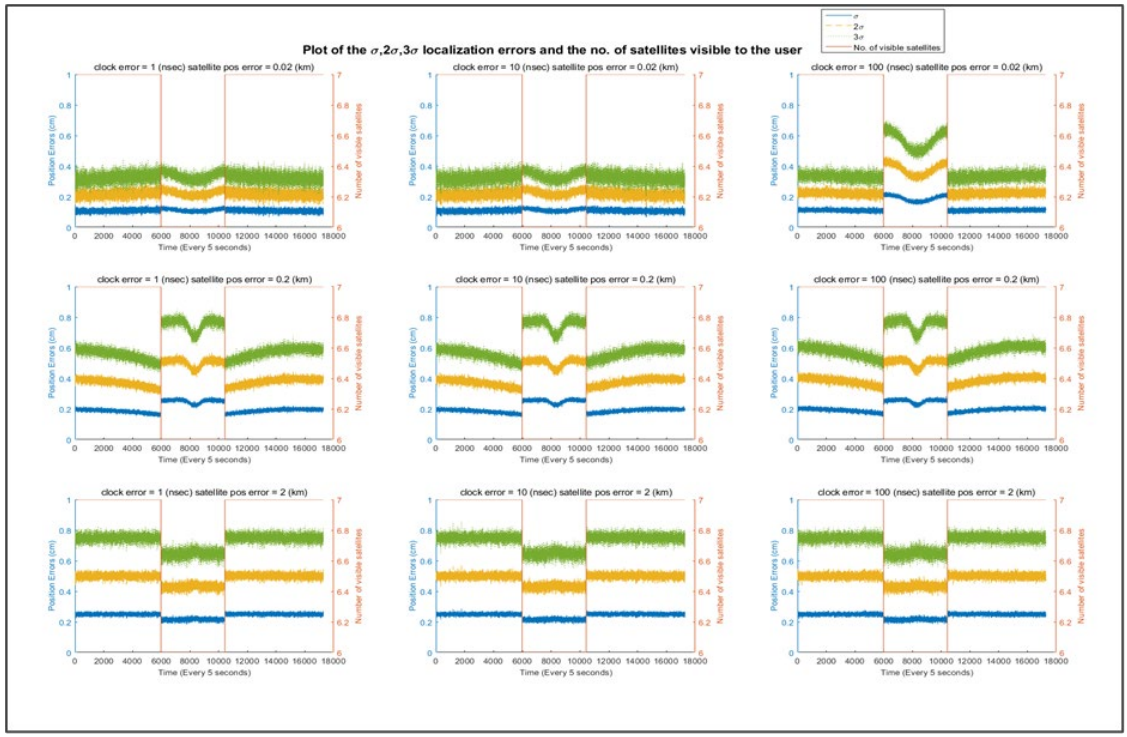

Figure 12: Plot of the position errors and numbers of L2SHO LCRNS satellites to the lunar surface user.

[§] Our team is collecting actual GNSS hardware specifications for modeling the clock error and incorporate it into the MATLAB LPNT simulator.

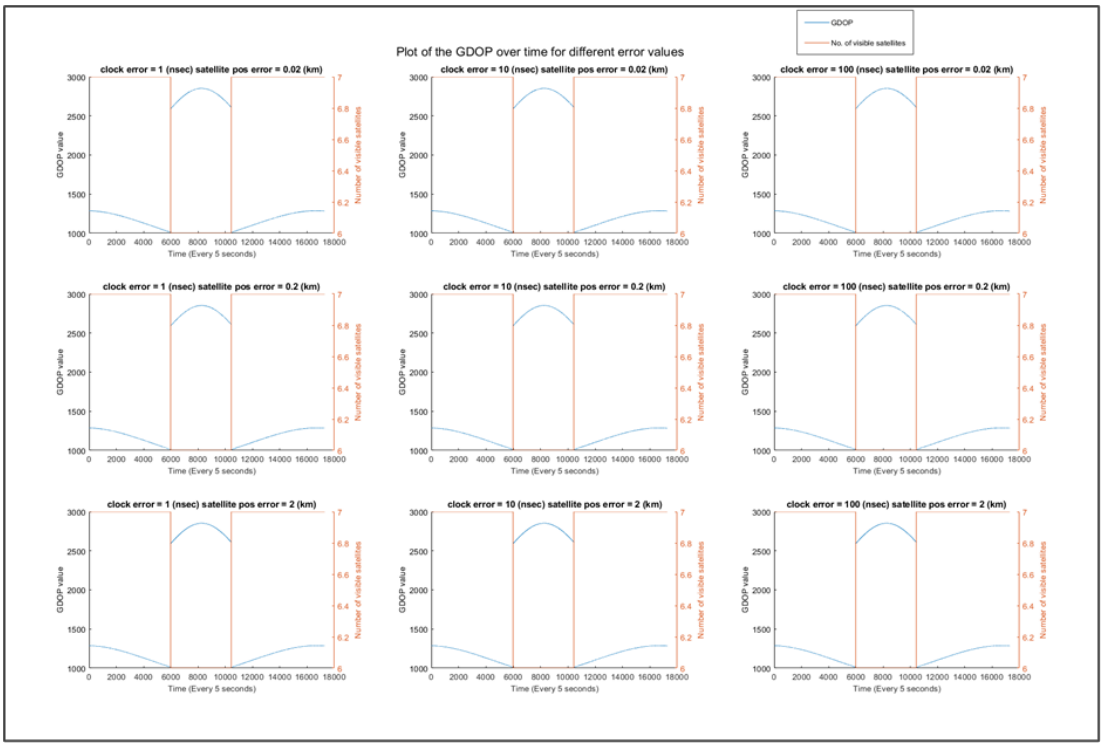

Figure 13: Plot of the GDOP and numbers of L2SHO LCRNS satellites to the lunar surface user.

9. CONCLUSION AND WAY FORWARD

This paper describes the IFT-CSUF team's approach for the design and development of our proposed MATLAB LPNT simulator that will be used in the assessment and evaluation of the feasibility of using a non-dedicated PNT service like GNSS for providing acceptable LPNT performance and desired services for future lunar missions, especially on the far side of the Moon. Using existing GPS, Galileo, QZSS, and planned LCRNS flying at L2 **S**outhern **H**alo **O**rbit, our simulation results show that the best L2SHO can provide 65% coverage of the lunar far-side with an average of 4.7 satellites in view every 5 seconds and a stability index of 1.00. The results also show that, for 10 LCRNS satellites at L2 Halo orbit, there is a minimum of 11 and a maximum of 15 GNSS satellites with a closed link over 24 hours. Our MATLAB simulator also explores and models the possibility of utilizing different orbital shapes for future far-side missions. To accurately predict the SNR received at L2SHO LCRNS from GNSS satellites, our team develops an accurate satellite attitude dynamic model with actual antenna patterns provided by the GNSS antenna suppliers that can be collected in the public domain. Since some of the GPS and Galileo antenna patterns are unavailable, our team derives the unknown patterns from the known ones using combined pattern recognition and interpolation approaches.

Currently, IFT-CSUF team is working on the enhancement of our LPNT end-to-end simulator by (i) continuing collecting data on actual GNSS antenna patterns and pointing models produced by antenna suppliers and incorporating them into the simulator, (ii) incorporating new MS&A models to predict time dilation because of signal “bending” in space, (iii) developing and incorporating various receive antenna models for L2SHO LCRNS for a trade study, (iv) developing innovative signal processing algorithms to improve the received SNR at LCRNS receiver, (v) incorporating actual hardware models used by actual GNSS transmitters (e.g., clock and frequency drift models), (vi) developing and incorporating User’s local position error estimation models as a function of received SNR, actual GNSS frequency and clock drift models, LCRNS receiver frequency and clock drift models, and selected GNSS constellation, and (vii) GDOP performance as a function of calculated (or predicted) User’s local position error estimation, actual GNSS frequency and clock drift models, and LCRNS receiver frequency and clock drift models. The IFT-CSUF team will also continue the Lunar Orbit MS&A effort to (i) incorporate alternative Halo orbit at Libration point L1, (ii) optimize LNSS satellite configuration to ensure continuous communication abilities with existing GNSS satellites, (iii) compute LCRNS for all satellite systems and explore LCRNS at L1 Halo orbit, and (iv) assess PNT performance for future Moon lander missions using non-dedicated PNT sources such as GNSS.

Acknowledgements

The authors thank Technical Communication Specialist Ms. Maria Rios from Intelligent Fusion Technology Inc. for her support in preparing this paper. This material is based upon work supported by the AFRL under Contract No. FA9453-23-P-A058. Any opinions, findings, conclusions, or recommendations expressed in this material are those of the authors and do not necessarily reflect the views of AFRL.

References

1. Comparison of Orbit Propagators. MATLAB & Simulink. Available at: https://www.mathworks.com/help/aerotbx/ug/comparison-of-orbit-propagators.html. Accessed April 14, 2024.
2. Galileo (Satellite Navigation). Wikipedia, Wikimedia Foundation, 23 Mar. 2024. Available at: en.wikipedia.org/wiki/Galileo_(satellite_navigation). Accessed 12 Apr. 2024.
3. GIS Geography (2024) *GPS accuracy: HDOP, PDOP, GDOP & Multipath, GIS Geography*. Available at: https://gisgeography.com/gps-accuracy-hdop-pdop-gdop-multipath/. Accessed: 10 April 2024.
4. Global Positioning System. Wikipedia, Wikimedia Foundation, 1 Apr. 2024, Accessed 12 Apr. 2024. en.wikipedia.org/wiki/Global_Positioning_System.
5. Grenier, A. *et al.* (2022) *Positioning and Velocity Performance Levels for a Lunar Lander using a Dedicated Lunar Communication and Navigation System*, *ResearchGate*. Available at: https://www.researchgate.net/publication/360377113_Positioning_and_Velocity_Performance_Levels_for_a_Lunar_Lander_using_a_Dedicated_Lunar_Communication_and_Navigation_System. Accessed: 13 April 2024.
6. Howell, K.C. (no date) *Three Dimensional, Periodic 'Halo' Orbits*, *1984, CeMec, page 53*. Available at: https://articles.adsabs.harvard.edu/cgi-bin/nphiarticle_query?bibcode=1984CeMec..32...53H&db_key=AST&page_ind=0&data_type=GIF&type=SCREEN_VIEW&classic=YES. Accessed: 12 April 2024.
7. Jun, W., Cheung, K.-M., Lightsey, E., & Lee, C. (2023). *Position, Velocity, and Timing for Lunar Descent and Landing with Joint Doppler and Ranging*. Jet Propulsion Laboratory, Pasadena, CA.
8. *Lunar Mission Analysis with the Orbit Propagator Block* (no date) *MATLAB & Simulink*. Available at: https://www.mathworks.com/help/aeroblks/lunar-mission-analysis-with-orbit-propagator-block.html. Accessed: 31 January 2024.
9. Other Global Navigation Satellite Systems (GNSS). GPS.Gov: Other Global Navigation Satellite Systems (GNSS). Available at: www.gps.gov/systems/gnss/#:~:text=Global%20navigation%20satellite%20system%20(GNSS,a%20global%20or%20regional%20basis. Accessed 12 Apr. 2024.
10. N. J. Bachman, "Reference Frames." NASA's Navigation and Ancillary Information Facility (NAIF), Revised: Dec. 2021. Accessed: April 24, 2024. Available:https://naif.jpl.nasa.gov/pub/naif/toolkit_docs/C/req/frames.html.
11. NORAD GP Element Sets Current Data. CelesTrak, celestrak.org/NORAD/elements/. Accessed 12 Apr. 2024.
12. Precision, Borealis. Step 1 - Satellites. GNSS Knowledge - Step 1 - Satellites - Borealis Precision - Industry Leading Representative, www.gnss.ca/gnss/1291-step-1-satellites. Accessed 12 Apr. 2024.
13. Quasi-Zenith Satellite System. Wikipedia, Wikimedia Foundation, 4 Mar. 2024, en.wikipedia.org/wiki/Quasi-Zenith_Satellite_System. Accessed 12 Apr. 2024.
14. *Three-body periodic orbits* (no date) *NASA*. Available at: https://ssd.jpl.nasa.gov/tools/periodic_orbits.html#/intro. Accessed: 12 April 2024.
15. Vaquero , M. and Senent, J. (no date) *Poincare: A multi-body, multi-system trajectory design tool*. Available at: https://indico.esa.int/event/224/papers/3852/files/225-Poincare_Vaquero.pdf. Accessed: 12 April 2024.
16. IOTA, What Is an Occultation?, May 31, 2023. https://occultations.org/occultations/what-is-an-occultation/.
17. N. 2 and Information, A.C. (2023) *Radio Link-budget calculations for ISM-RF products*, *Analog Devices*. Available at: https://www.analog.com/en/resources/ technical-articles/radio-linkbudget-calculations-for-ismrf-products.html. Accessed: 23 May 202)
18. Steigenberger, P., Thoelert, S. and Montenbruck, O. (2017) Journal of Geodesy, 92(6), pp. 609–624. Doi: 10.1007/s00190-017-1082-2.

19. Steigenberger, P., Thoelert, S. and Montenbruck, O. (July 2017) Measuring GNSS Satellite Transmit Power.